Influence of soil deformability on the seismic response of a masonry tower

Siro Casolo[1] · **Vito Diana**[1] · **Giuseppina Uva**[2]

Received: 21 May 2016 / Accepted: 29 November 2016 / Published online: 17 December 2016

1 Introduction

The dynamical modelling of seismic response of masonry towers presents some special features compared to what is usually done for ordinary building. Firstly, it should be considered that the static stress due to gravity loads, i.e. the vertical compressive stress component, may be already close to the limit strength of the masonry material (Binda et al. 1992). The phenomenology of the damage mechanisms depends on the relative importance of bending, shear an axial action as well as on the boundary conditions, which are essentially given by the elastic characteristics of the foundation soil. Damage due to the bending moment is manifested by crack opening and compressive crushing at the base of the tower. Shear damage tends to be widespread in the central part of the tower, and is often announced by some vertical cracks starting at openings (Lourenço 2002; Pena et al. 2010). The vertical seismic loading, moreover, tend to have an effect that influences both the bending and the shear behavior. Actually, the increase of vertical compression stress component can trigger the collapse of the material for crushing, while it also modifies the shear strength of the material, which is related to the internal friction of the masonry. In general, the first natural mode dominates the dynamic response of this type of structure. However, the empirical evidence (Doglioni et al. 1994) as well as some computational studies (Casolo et al. 2013), show many cases of slender towers, which suffered significant damages to be attributed to the second bending mode of vibration (Curti et al. 2006). In these cases, the damage is concentrated in the top part of the tower, also in combination with the structural weakening determined by the presence of the belfry (Milani et al. 2012). The structure of the towers is quite simple, from a geometric point of view, so that in some cases it can be assimilated to a simple beam constrained to the ground.

Frequently, research studies about the dynamic response of masonry towers by Finite Elements perform a very detailed numerical modelling of the structure, while a perfect fixed constraint at the base is assumed (Acito et al. 2014; Milani and Valente 2016). This approximation is correct if the foundation soil has the elastic features of a compact rock, otherwise it can lead to an inaccurate estimation of the crack pattern, because of effects related to the 2nd natural mode and to the vertical component of acceleration (Casolo and Uva 2013; Ivorra et al. 2016). A proper modelling of boundary conditions (namely, the volume of soil around the foundation), is a critical aspect of the implementation of computational models aimed at the dynamic analysis of structures like masonry towers (Kouroussis et al. 2011; Kuhlemeyer and Lysmer 1973). Clearly, when the aim is the determination of damage patterns, it is necessary to implement a numerical model endowed with a suitable geometric detail and also with a sufficiently refined constitutive model, able to describe the damage response of masonry material. Unfortunately, it is very difficult to manage within a single, complete model, also an adequately refined description of the foundation soil (Burban et al. 2010; Camata et al. 2008).

The present research study investigates the impact of the dynamic interaction between the tower and the soil on the towers' damage through a rather sophisticated numerical

✉ Siro Casolo
siro.casolo@polimi.it

[1] Department of Architecture, Built Environment and Construction Engineering, ABC, Politecnico di Milano, Piazza Leonardo da Vinci 32, 20133 Milan, Italy

[2] Department DICATECh, Politecnico di Bari, Via E. Orabona 4, 70125 Bari, Italy

modelling. Being aware that is not possible to present an exhaustive study that covers all the possible tower types, we have focused the attention on a case model characterized by average features with regards to the geometry as the mechanical characteristics. Moreover, we have circumscribed the field of study by focusing on three aspects: (1) alteration of the ground motion due to the presence of the tower; (2) relative importance of higher vibration modes; (3) importance of the vertical component of the ground acceleration. The problem is described by means of a three-dimensional finite element approach; the constitutive modelling includes non-linear mechanical characteristics with the possibility of damage (Lee and Fenves 1998; Lubliner et al. 1989); the lateral boundaries of soil is modelled by elastic *infinite elements*, characterized by non-reflecting boundaries in order to represent the far-field behavior (Lysmer and Kuhlemeyer 1969; Yerli et al. 2003; Zienkiewicz et al. 1983, 1985).

2 Case study and model adopted

An ideal case study is considered which represents the main features of many recurring bell towers present in the seismic areas of Northern Italy. This case model is supposed to be structurally independent from other buildings, and characterized by regular geometric configuration both in plan and in elevation. The geometry of the model is quite simplified, and the dimensions were chosen by analyzing a series of representative examples (Doglioni et al. 1994; Casolo 1998; Casolo et al. 2013; Bartoli et al. 2016). Figures 1 and 2 shows the axonometric, plan views of the tower, while the main dimensions are summarized in Table 1.

The 3D FEM model of the tower is implemented using the computer code *Abaqus 6.14* and consists of 22,528 nodes and 103,532 four-node linear tetrahedral elements (Abaqus element Code: *C3D4*) (ABAQUS 2014).

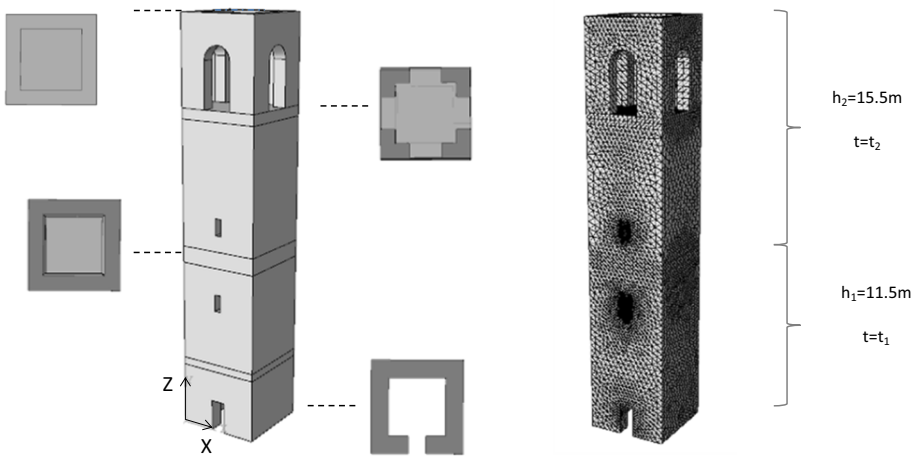

Fig. 1 3D model of the masonry bell tower and FEM discretization

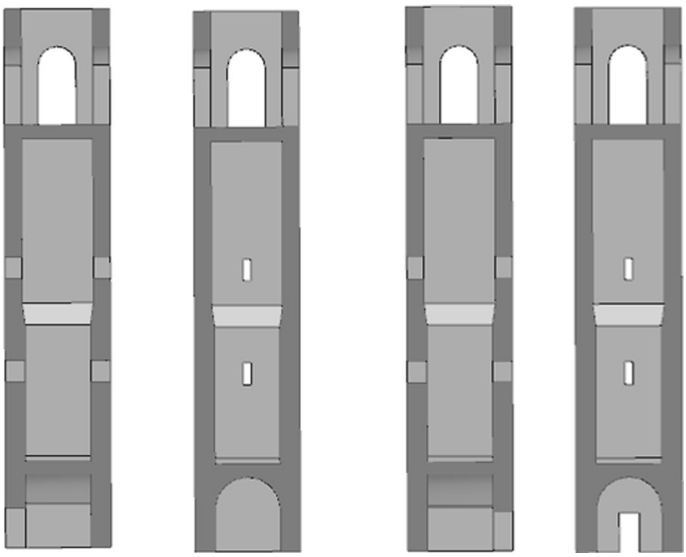

Fig. 2 Schematic views of the 3D model of the masonry bell tower

Table 1 Geometrical details of the masonry tower

Total height ($h = h_1 + h_2$)	27 m
Base dimensions L × L	5.30 m × 5.30 m
Masonry thickness	$t = t_1 = 1.00$ m
	$t = t_2 = 0.85$ m

2.1 Soil modeling as unbounded domain

The study of the interaction between the tower and the soil (SSI) falls in the set of problems in which the region of interest is small when compared with the surrounding medium. In theory the discretization should be extended to a distance where the influence of the surrounding medium on the region of interest can be neglected. This approach requires a high computational cost, the test of several mesh extensions, and sometimes the correct boundary condition is not even achievable. In the static field, the problem is easy to solve: the distance at which there is not a significant stress variation produced by the disturbing load is straightforwardly derived, and the selection of appropriate kinematic constraints is usually enough in order to guarantee correct results (for example, the inclusion of sliders on the border side of the ground). On the other side, a correct modeling of the domain limits is crucial in dynamic analysis, since the mesh boundary can reflect the elastic energy back to the region of interest. Basically, one major problem that is encountered in the study of the dynamic behavior of soil-structure systems subjected to seismic forcing (and more in general in the simulation of wave propagation phenomena) concerns the possible occurrence of multiple reflections in correspondence of the outer contours of the model. These reflected waves have no real physical correspondence, and represent a potential source of error in the solution. An innovative approach employs the *infinite elements*, which are defined in semi-infinite

domains and endowed with decay functions suitably selected for static conditions (Zienkiewicz et al. 1983) and for dynamic conditions (Lysmer and Kuhlemeyer 1969). These elements, suited for modeling the far-field region, are used in combination with standard finite elements by which instead is modeled the area of interest. The dynamic response of the infinite elements is based on theoretical considerations about the particular case of waves propagating in the direction orthogonal to the boundary plane on which we want to eliminate the reflections. Considering a one-dimensional problem, if y is the direction of propagation and x is the direction of the tangent to the contour surface of the near-field region, the stress conditions on the contour surface, which will be imposed at the node level in the FE model, are:

$$\sigma_{xy} = \tau = a\rho V_S \frac{\partial u_x}{\partial t} \tag{1}$$

$$\sigma_{yy} = \sigma_n = b\rho V_P \frac{\partial u_y}{\partial t} \tag{2}$$

where V_S and V_P are the propagation speeds of S-waves and P-waves, respectively, in a medium with density ρ; a and b are coefficients ranging from 0 (free boundary) to ∞ (rigid border); $\dot{u}_x = \frac{\partial u_x}{\partial t}$ and $\dot{u}_y = \frac{\partial u_y}{\partial t}$ are the velocities at the interface between the near-field and the far-field region. When the coefficients a and b are far from the extremes of their definition range, Eqs. (1) and (2) express that the tangential stress τ is proportional to the x component of the velocity, $\dot{u}_x$ and the normal stress σ_n is proportional to the y component of the velocity $\dot{u}_y$, that is to say, the contour surface is a perfect "transmitter". In the one-dimensional case previously discussed, the radiation conditions (1), (2) prove to be accurate. However, this technique has been used successfully also in 2D and 3D conditions. In our 3D FEM model of the masonry tower and soil, the elastic layer consists of 11,459 nodes and 53,178 elements (ABAQUS 2014). The portion of the soil considered for the near-field volume is characterized by a height H equal to 25 m and a width W of 200 m (W = 8H) in order to avoid interference or absorption of energy by the infinite region. The height of the soil layer has been chosen in order to minimize the eventuality of resonance and multiple reflections of the waves (Casolo and Uva 2013): $\frac{V_S}{4H} = f_I$ (f_I = frequency of the first natural mode of the tower which is about 2 Hz). Thence, for the two considered soil types, we obtain the following height values:

$$\frac{V_{S_{soil\,1}}}{4f_I} = H_1 = 34\,\text{m}; \quad \frac{V_{S_{soil\,2}}}{4f_I} = H_2 = 81\,\text{m} \tag{3}$$

The nodal displacements at the base of the soil layer (bedrock) have been fully constrained, whereas the *infinite elements* were adopted for the correct description of the behavior of the far-field zone (Fig. 3) both in the static and dynamic field, as previously illustrated. Considering that masonry bell-towers are usually built within urban contests, we have deemed that the cases of compact rock and loose sand or soft clay are scarcely representative (the former is a rare case, in an urban contest; the latter would require a different foundation). We have thence limited the range by selecting two types of soil, characterized by different deformability, in order to represent a compact gravel and a medium dense sand or medium stiff clay. The mesh size is progressively refined in order to achieve a greater accuracy near the tower foundation.

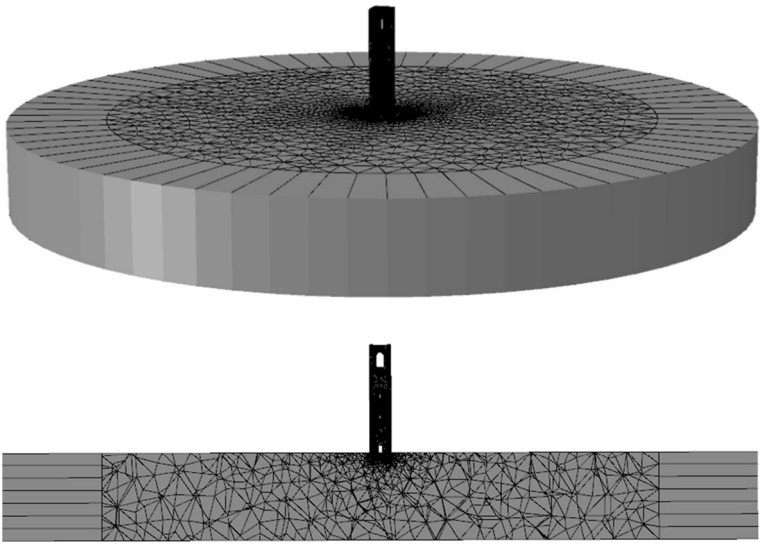

Fig. 3 FEM 3D model, section view of the tower–soil system with *infinite elements* in Abaqus

2.2 The tower–soil system

After implementing the individual FE models for the masonry tower and for the soil substrate, they have been assembled within a single complete model, as shown in Fig. 3. The foundation of the tower has a square base (6.8 m × 6.8 m) and is 2.5 m high. The overall model is thus made of 33,782 nodes and 156,710 elements, of which 588 Hexahedral infinite elements (CIN3D8) and 156,122 linear tetrahedral elements (C3D4). In order to simulate the soil-structure interaction, the interface between the foundation and the elastic soil substrate has been modeled by adopting a *master–slave* modeling. A *Penalty* type interaction law was defined for the tangential behavior and a *Hard contact* type law for the normal behavior, in order to prevent interpenetration between contact surfaces.

2.3 Mechanical parameters of the materials

2.3.1 Soil

The two soils characterized by different deformability (according to Par 2.1), will be hereafter denoted by soil I and soil II. Soil is modeled in a simplified way, as a linear elastic layer with Rayleigh damping and the relevant constitutive parameters are summarized in Table 2 (Kramer 1996).

2.3.2 Masonry constitutive model

It is well-known that the dynamic response of masonry structures is characterized by a great complexity because of the composite nature of materials and the non-linearity involved. Different computational approaches can be adopted to face the analyses, as shown in the related scientific literature, which is huge (Lourenço 2002). In this research work, masonry has been modeled as a continuous homogeneous material, suitably

Table 2 Mechanical parameters adopted for the two types of soil

	E (MPa)	ν	ρ (kg/m^3)	V_s (m/s)	α_R	β_R
Soil I	280	0.2	1800	270	1.170	0.002
Soil II	1400	0.2	1800	646	2.637	0.001

α_R and β_R are the coefficients governing the Damping Rayleigh matrix: $\alpha_R = \xi \frac{2\omega_i\omega_j}{\omega_i+\omega_j}$ $\beta_R = \xi \frac{2}{\omega_i+\omega_j}$

ω_i and ω_j are the angular natural frequencies of the modes i and j, while ξ is the equivalent viscous damping

discretized according to a variable mesh of tetrahedral finite elements. The parameters that have been chosen for the tower are shown in Table 3.

For the constitutive modelling of masonry in the non-linear field, the *Concrete Damage Plasticity* material model (CDP) has been adopted (Lee and Fenves 1998; Lubliner et al. 1989). Although originally conceived to describe the non-linear behavior of concrete, this model can be accepted for masonry (Barbieri et al. 2013; Milani and Valente 2015; Giresini 2016), as long as appropriate parameters are adopted. In fact, even if CDP cannot account for the orthotropy of the material, it allows for model distinct tensile and compressive strength, as the case of masonry, with distinct damage parameters in tension and compression. The yield function used is a modified Drucker–Prager one, controlled by the hardening variables $\tilde{\varepsilon}_c^{pl}$ and $\tilde{\varepsilon}_t^{pl}$ (equivalent plastic deformation in compression and in tension, respectively). The CDP Model includes the parameters α and K_c, which are particularly important in the description of the nonlinear behavior of the material. These parameters govern the shape of the yield surface in the deviatoric plane. In particular, the value $K_c = 1$ identifies the circular section of Drucker–Prager model, whereas for $K_c < 1$, the shape of the yield surface becomes more similar to a triangle with curved sides as much as K_c moves away from the unity (Fig. 4). In the model, the objective was to assume a yield surface that could approximate as much as possible a Mohr–Coulomb criterion in the deviatoric plane. This has been obtained by assuming the following values for the CDP Model parameters: $\alpha = 0.12$, $K_c = 0.667$. The constitutive model is characterized by non-associated plastic flow condition. Actually, by observing the Lee and Fenves yield function in the deviatoric plane, we can notice that there are critical corner points due to the fact that the plastic deformation cannot be univocally determined by using an associated flow. The non-associated flow law of the model is:

$$\dot{\bar{\boldsymbol{\varepsilon}}}^{pl} = \dot{\lambda} \frac{\partial G(\bar{\boldsymbol{\sigma}})}{\partial \bar{\boldsymbol{\sigma}}} \tag{4}$$

with the Drucker–Prager hyperbolic plastic potential given by:

$$G = \sqrt{(\varepsilon \sigma_{to} \tan\psi)^2 + \bar{q}^2} - \bar{p} \tan\psi \tag{5}$$

where ε is the eccentricity, and represents the rate at which the function approaches the asymptote, while ψ is the dilatancy angle in the plane $\bar{p} - \bar{q}$ at high confining pressures.

Table 3 Mechanical parameters adopted for the masonry tower

E (MPa)	ν	ρ (kg/m^3)	α_R	β_R
3500	0.1	1900	0.992	0.001

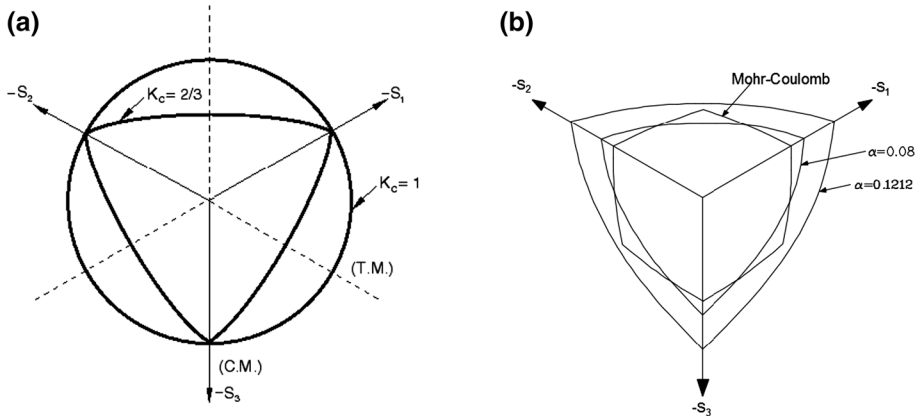

Fig. 4 **a** Yield surfaces in the deviatoric plane for different values of the parameter K_c. **b** Yield surfaces in the deviatoric plane for $K_c = 0.667$, considering different values of α

Table 4 Values of the masonry mechanical parameters adopted for the numerical simulations

ψ (°)	ε	σ_{b0}/σ_{c0}	K_c	λ
15–25	0.1	1.16	0.667	0.00001

The fact of considering non-associated plastic flow through a hyperbolic function also allows to easily control the phenomenon of dilatance, which is dependent on $\bar{p}$. The dilatancy angle is assumed to be a function of the confining pressure (Van Der Pluijm 1993) existing at different levels of the tower, and is variable between 15 degrees (foundation) and 25 degrees (belfry). A further parameter of viscosity λ was added to the model in order to obtain a visco-plastic regularization that improves the convergence of the model in softening conditions. The model parameters used are shown in Table 4.

The post-elastic behavior in tension and compression is defined by a uniaxial stress–strain relationship and by a law of variation of the scalar damage variable[1] such that (ABAQUS 2014):

$$\sigma_c = (1 - d_c)E_0\left(\varepsilon_c - \tilde{\varepsilon}_c^{pl}\right) \tag{6}$$

$$\sigma_t = (1 - d_t)E_0\left(\varepsilon_t - \tilde{\varepsilon}_t^{pl}\right). \tag{7}$$

where ε_t is the total tensile strain, ε_c is the total compressive strain, and σ is the Cauchy stress, thus $\bar{\sigma} = \frac{\sigma}{(1-d_t)}$ is the effective stress. The uniaxial law in tension is assigned as a function of the cracking deformation (cracking strain), which is defined as the total tensile strain minus the elastic strain corresponding to the undamaged material:

$$\tilde{\varepsilon}_t^{ck} = \varepsilon_t - \varepsilon_{0t}^{el} \tag{8}$$

[1] The scalar damage variable d (d_c in compression and d_t in tension) is representative of the stiffness degradation of the material, thus $(1 - d)$ is the ratio of the effective load-carrying area (i.e., the overall area minus the damaged area) to the overall section area.

Also the tensile damage function $d_t = d_t\left(\tilde{\varepsilon}_t^{pl}\right)$. will be assigned in terms of $\tilde{\varepsilon}_t^{ck}$. The cracking deformation is then converted into plastic deformation in accordance with the relation:

$$\tilde{\varepsilon}_t^{pl} = \tilde{\varepsilon}_t^{ck} - \frac{d_t}{(1-d_t)}\frac{\sigma_t}{E_0} \tag{9}$$

The uniaxial law in compression is instead assigned as a function of the inelastic deformation (crushing strain), that is defined as the total compressive strain minus the elastic strain corresponding to the undamaged material:

$$\tilde{\varepsilon}_c^{in} = \varepsilon^c - \varepsilon_{0c}^{el} \tag{10}$$

Similar considerations apply to the compressive damage function $d_c = d_c\left(\tilde{\varepsilon}_c^{pl}\right)$, with:

$$\tilde{\varepsilon}_c^{pl} = \tilde{\varepsilon}_c^{in} - \frac{d_c}{(1-d_c)}\frac{\sigma_c}{E_0} \tag{11}$$

Under cyclic loading, it is necessary to introduce specific corrections to take into account the possible recovery of stiffness that is expected in correspondence of a load reversal. In fact, in these conditions, the degradation mechanism is more complex, and should take into account that the effect of the opening and closure of existing micro-cracks over the slope of the unloading/reloading branches. This effect, known for quasi-brittle materials as *unilateral effect*, is significant in the transition from tension to compression and not vice versa, since the transition from the compressive region to the tensile one sees a quick reopening of the cracks that had already formed during the previous cycle. The stiffness recovery parameters under cyclic actions, respectively under tension and compression, are called w_t and w_c, and in the model they have been assumed equal to 0 and 1, coherently with the previous considerations (Fig. 5). The uniaxial stress–deformation relationship and the variation law of the damage variable assumed in compression and in tension are specified in Tables 5 and 6.

The damage parameters d_c and d_t have been assumed as 0.95 at the deformations corresponding to the residual uniaxial stress value in tension and compression, respectively. Therefore, the elastic stiffness assumes a value equal to 5% of the initial one in correspondence of such values of strain.

3 Preliminary frequency analysis

At preliminary, modal analysis has been carried out with the aim of studying the influence of the elastic modulus of the soil substrate on the dynamic response of the tower in the linear field. Besides the bell tower–soil system (complete model—Par. 2.2), also the limit case of the tower with an ideal base constraint (cantilever scheme) has been analyzed, which allows to make some interesting comparisons. For the cantilever scheme, the results of the analyses in terms of deformed shapes and frequency values (expressed in Hz) are shown in Fig. 6 and Table 7 (since the tower is symmetric, flexural modes are reported only for the x direction (Gentile et al. 2015; Ivorra and Pallares 2006).

As previously mentioned, two different conditions of soil deformability are considered in the complete model (soil I, E = 280 MPa; soil II, E = 1400 MPa). The numerical

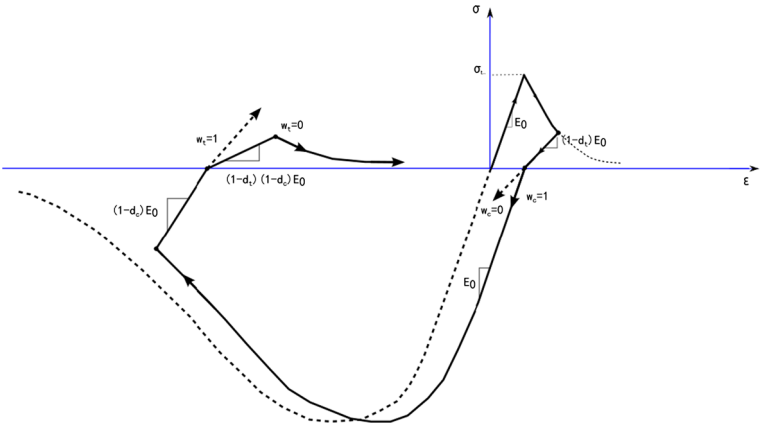

Fig. 5 Effects of the stiffness recovery parameters w_c and w_t on the uniaxial hysteretic behaviour

Table 5 Uniaxial stress–strain values utilized in the CDP model for masonry

σ_t (MPa)	$\tilde{\varepsilon}_t^{ck}$
0.2	0
0.02	0.0025
0.02	0.01
σ_c (MPa)	$\tilde{\varepsilon}_c^{in}$
2	0
2	0.0015
0.2	0.005
0.2	0.1

Table 6 Scalar damage values utilized in the CDP model for masonry

d_t	$\tilde{\varepsilon}_t^{ck}$
0	0
0.95	0.0025
d_c	$\tilde{\varepsilon}_c^{in}$
0	0
0.95	0.005

analysis of the individual soil layers (without the tower) has provided the values of the 1st natural frequencies for each of them, which are respectively equal to 2.70 and 6.46 Hz.

Modal analyses have then been performed for the complete model in each of the two soil cases (Figs. 7, 8). As described in Par. 2.2, the FE model of the substrate layer provides fixed constraints at the base and *infinite elements* along the lateral boundaries.

By analyzing the results of modal analyses, (also reported in Table 8 and in Fig. 9 which shows a direct comparison among the modal shapes obtained), the following considerations can be made:

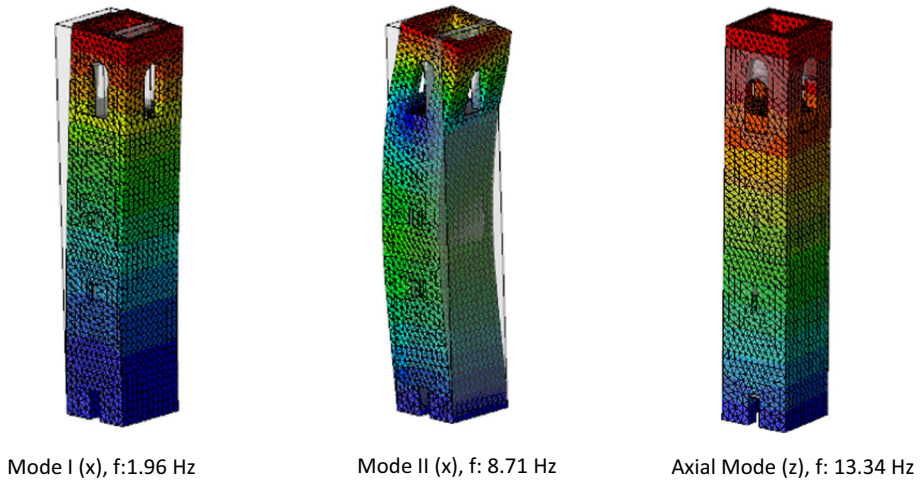

Fig. 6 Natural modes of the cantilever scheme in the x direction and relative frequencies

Table 7 Results of the modal analysis for the Cantilever model of the masonry tower

Mode	Period (Hz)	Type	Excited mass m_x%	Excited mass m_y%	Excited mass m_z%
1	1.95	1st flexural	0.006	58.425	0.007
2	1.96	1st flexural	58.442	0.007	0
3	7.83	1st torsional	0.295	0	0
4	8.71	2nd flexural	21.125	0.002	0
5	8.75	2nd flexural	0.002	20.868	0
6	13.3	1st axial	0	0	78.876

- The 1st natural frequency of the cantilever scheme is lower than those of the individual soil layers. Consequently, the 1st natural mode of the combined bell tower–soil system is ruled by the motion of the bell tower.
- The frequency of the 2nd natural mode of the cantilever scheme is higher than the 1st natural frequency of the soil layers. As a result, soil always participates to the 2nd modal shape of the bell tower–soil system. In any case, the decrease of the substrate deformability reduces such effect.
- In the bell tower–soil system (for both soil types), the 1st mode exhibits an interaction effect at the base of the tower that can be described by a rotational spring with a stiffness proportional to the elastic modulus of the soil. For the 2nd natural mode, instead, the interaction effect can be clearly visualized as a roto-translational spring. The translational component (Rigid translation) is more evident than the rotational one (Rocking) and it is clearer with the decrease of the elastic layer stiffness. Moreover, it is worth noting that for soil I, the rigid translation is much larger than for soil II, and more important for the second mode (Fig. 9).
- The ratio of the natural frequencies of the complete models to the corresponding cantiler values[2] (η) decrease with the increasing of the soil deformability, faster for the

[2] $\eta = f_{ij}/f_{0j}$. The first index denotes the Id of the FE model considered, whereas the second index denotes the natural mode.

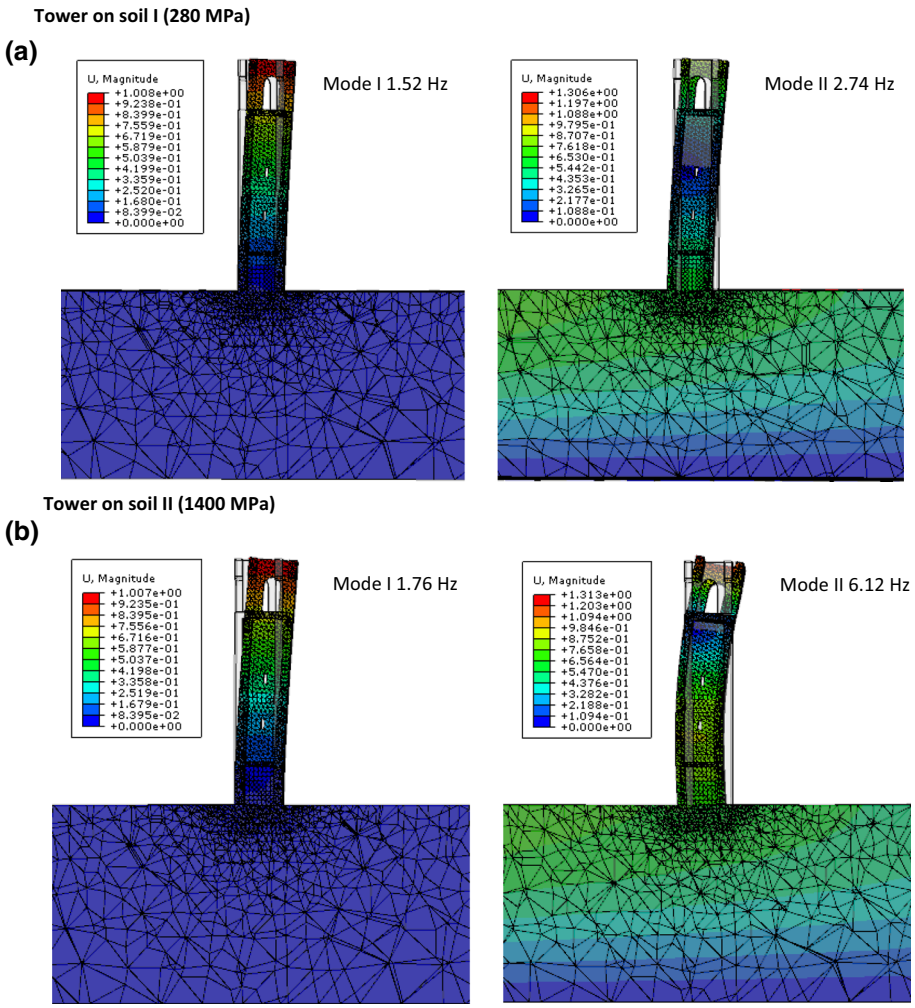

Fig. 7 Results of modal analysis for the complete model. **a** Tower on soil I: 1st and 2nd natural mode in x direction; **b** tower on soil I: 1st and 2nd natural mode in x direction

second mode respect to the first natural mode. In fact, the second natural mode frequency decreases of 69% ($\eta = 0.31$) when passing from cantilever conditions to tower on soil I conditions, instead the frequency of the first natural mode decrease only of 22% ($\eta = 0.78$). Moreover the ratio of the first natural frequency to the second one[3] (α) increase with the soil deformability (Table 8; Fig. 9). It is apparent that the second natural mode of the tower is influenced by soil deformability much more than the first mode. These results accord with (Luco et al. 1988, Veletsos and Meek 1974).

In Fig. 8 it can be observed that all the natural axial modes are characterized by a very reduced frequency if compared to the corresponding natural modes of the cantilever model. For the tower on soil I there is a clear reduction in the frequency, attributable to the

[3] $\alpha = f_{i1}/f_{i2}$.

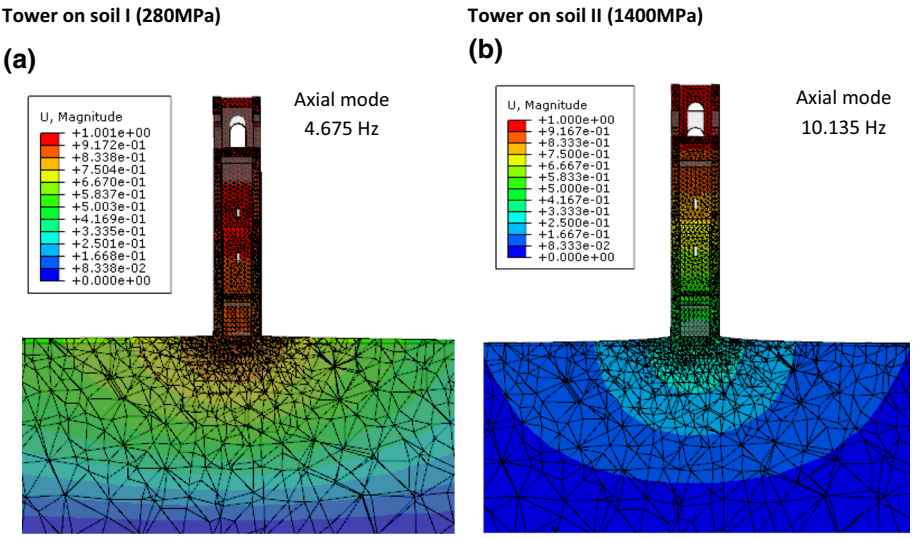

Fig. 8 **a** First natural mode in the z direction for the tower on soil I, **b** first natural mode in the z direction for the tower on soil II

Table 8 Synopsis of the results from the modal analysis in the different models

Id	Model	Natural mode	Frequency (Hz)	$\eta = f_{ij}/f_{0j}$	$\alpha = f_{i1}/f_{i2}$	δ, rigid translation (mm)	θ, rocking (10^{-4} °)
0	Cantilever	1	1.95	1	0.22	0.000	0.000
		2	8.71	1		0.000	0.000
1	Tower–soil 2 (1400 MPa)	1	1.76	0.91	0.29	0.005	1.987
		2	6.12	0.70		0.579	5.503
2	Tower–soil 1 (280 MPa)	1	1.52	0.78	0.55	0.024	6.758
		2	2.74	0.31		0.651	9.945

relevant deformability of the soil which shows a very different behavior from full constrain (Ivorra et al. 2010).

In order to obtain also a quantitative estimation of differences in modal shapes between the natural modes of the cantilever model and the natural modes of the tower–soil models the MAC values (Modal Assurance Criterion) have been calculated.[4] If $\{\varphi_A\}_r$ and $\{\varphi_B\}_q$ are two modal shape vectors referred to the natural modes r and q of the reference models A and B, the scalar defined as:

$$MAC(r,q) = \frac{\left|\{\varphi_A\}_r^T \{\varphi_B\}_q\right|^2}{\left(\{\varphi_A\}_r^T \{\varphi_A\}_r\right)\left(\{\varphi_B\}_q^T \{\varphi_B\}_q\right)} \tag{12}$$

[4] The modal shapes are previously depurated from rigid-body motions and then normalized to unity at the top of the structure.

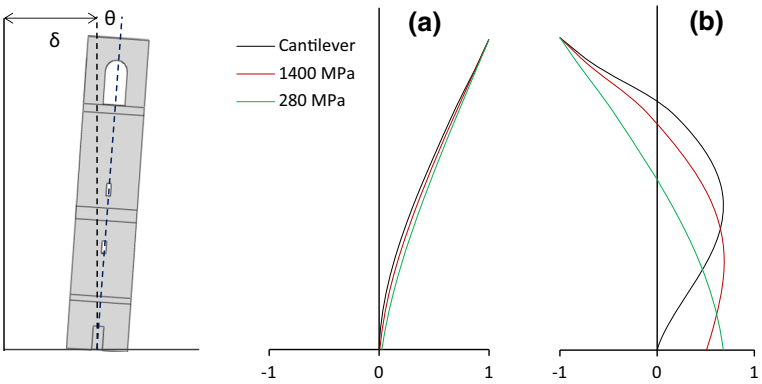

Fig. 9 **a** First and second, **b** normalized natural modes in the x direction for the three tower models (preserving the rigid translation δ and rocking θ)

is an indicator sensitive to large differences and relatively insensitive to small differences in the modal shapes which assess their degree of consistency (Allemang and Brown 1982).

The resulting scalars are arranged into the CrossMAC matrix (Table 9) which shows that the 1st natural modes of all the three tower models are consistent. Instead, the 2nd natural modes of the bell tower–soil systems are rather different from the cantilever one. In particular, while the 2nd mode of the tower–soil II has a good degree of correspondence with that of the Cantilever model, this latter and the second mode of the tower on soil I are almost unrelated. Moreover, we can note a high degree of correlation between the 2nd natural mode of tower–soil I system and the 1st mode of the Cantilever model.

4 Definition of the seismic action

The non-linear dynamic analyses have been performed by using (as seismic input) two groups of natural accelerograms. The first group refers to the recordings of the earthquake that hit Emilia-Romagna region in May 2012, the second one refers to the Friuli Earthquake of September 1976. In particular, we have chosen the main shock of May 29, 2012 at 09:00, recorded at the station MIR02 located in Mirandola (MO), and that recorded on September 15, 1976 at 05:15 in the GMN station, located in the town of Gemona (UD) (Luzi et al. 2008; Pacor et al. 2011; ITACA working group 2016). The acceleration time-histories are shown in Fig. 10. These seismic events are substantially different. The strong ground motion recorded at Mirandola, have high energy contents concentrated at high frequencies if compared to those of Gemona, even if the latter has a higher peak ground acceleration and velocity (as will be shown in the next section). In view of the dynamic analyses, it is worth observing that the accelerograms will be assigned at the base of the elastic soil layer, in order to obtain the realistic conditions of plane wave propagation.

However, if one need to perform a comparison on equal terms among the dynamic responses of the structure subjected to different support conditions, it is necessary that the seismic excitation at the base of the tower is the same for each of the compared situations (namely, substrates with different deformability). To this aim, it is necessary to assign at the base of the substrate

Table 9 Mac values between the natural modes of the cantilever model and the natural modes of the complete models

Model	Mode	Tower–soil II (1400 MPa)		Tower–soil I (280 MPa)	
		1	2	1	2
Cantilever	1	0.984	0.619	0.977	0.889
	2	0.0011	0.453	0.0018	0.066

layer a specific accelerogram, properly processed according to each analysis case, so that the resulting signal at the base of the tower is always the same, for all cases.

The following numerical procedure has been adopted in order to obtain this objective:

- The original accelerogram[5] is assigned at the substrate base of the 3D soil model, and the resulting signal at the surface is recorded.
- For the two types of soils, transfer functions are derived (for S-waves and P-waves), in the following way: If a(t) is the accelerogram assigned to the bedrock, $a^*(t)$ is the signal recorded at a height $z = 0$ and $\mathrm{FT}[a^*(z = 0,f)]$ and $\widetilde{\mathrm{FT}}[a(z = H,f)]$ are respectively the Fourier transform (FT) of $a^*(t)$ and the regularized (*water level regularization*) Fourier Transform[6] of a(t), then the transfer function *TF*(*f*) is:

$$TF(f) = \frac{\mathrm{FT}[a^*(z = 0,f)]}{\widetilde{\mathrm{FT}}[a(z = H,f)]} \tag{13}$$

  which is a complex function that describes the relationship between the Fourier transforms of the acceleration at the base and the one at the surface of the elastic layer. With z we indicate the height measured from the surface, f is the frequency in Hz.
- After deconvolution, it is possible to calculate, for each type of elastic substrate, the accelerogram that should be assigned at the bottom in order to induce at the surface the desired acceleration record, that is to say, in our case, the three components of the Mirandola and Gemona strong ground motions of the ITACA database:

$$FT[a^{**}(z = 0,f)] = \frac{\mathrm{FT}[a(z = H,f)]}{\widetilde{TF}(f)} \tag{14}$$

[5] The accelerograms of ITACA database, shown in Fig. 10.

[6] In Eq. (13), if the denominator is $\mathrm{FT}[a(z = H,f)]$ one may have values zero or very close to zero (at least for some frequencies), causing many spikes. A water-level regularization (Clayton and Wiggins 1976) can reduce this phenomenon, by introducing a scalar value w (called critical level) and adjusting $\mathrm{FT}[a(z = H,f)]$ only when its modulus is lower than w. Thus it is possible to write:

$$\widetilde{\mathrm{FT}}\,[a(z = H,f)] = \begin{cases} FT[a(z = H,f)], & if\ |\mathrm{FT}[a(z = H,f)]| > w \\ w\dfrac{\mathrm{FT}[a(z = H,f)]}{|\mathrm{FT}[a(z = H,f)]|}, & if\ 0 < |\mathrm{FT}[a(z = H,f)]| \le w \\ w, & if\ |\mathrm{FT}[a(z = H,f)]| = 0 \end{cases}$$

where $\widetilde{\mathrm{FT}}[a(z = H,f)]$ is the regularized Fourier Transform of $a(z = H,f)$. The same considerations are referred to *TF*(*f*) in Eq. (14).

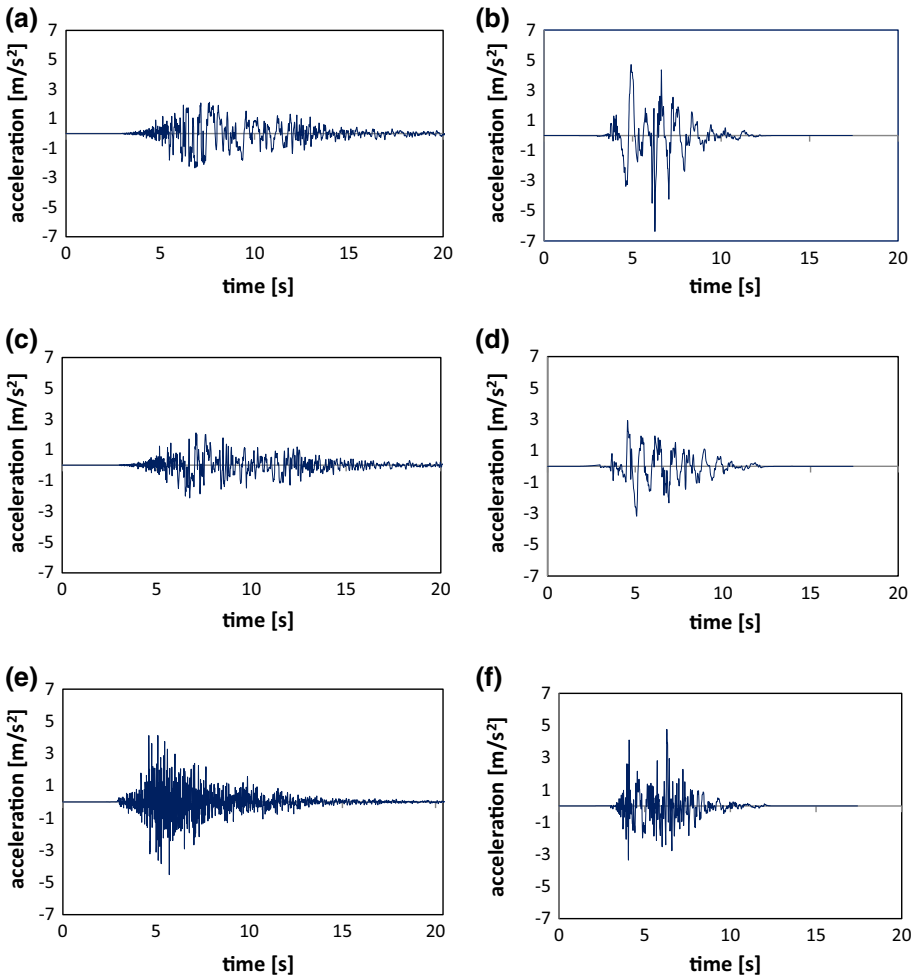

Fig. 10 Mirandola accelerogram, component X (**a**), Y (**c**), Z = vertical (**e**); Gemona accelerogram, component X (**b**), Y (**d**) and Z = vertical (**f**)

where $FT[a^{**}(z=0,f)]$ is the Fourier transform of the unknown accelerogram $a^{**}(t)$ and $\widetilde{TF}(f)$ is the regularized transfer function TF(*f*). Therefore, the accelerograms we are searching for will be obtained by inverse Fourier transform (IFT):

$$IFT\left[\frac{FT[a(z=H,f)]}{\widetilde{TF}(f)}\right] = IFT\{FT[a^{**}(z=0,f)]\} = a^{**}(t) \tag{15}$$

Since we consider all the three components of Mirandola and Gemona ground motion, the accelerograms obtained by deconvolution for the two soils are 12 in total, three for each type of elastic layer and seismic event considered.

5 Dynamic analyses

5.1 Linear dynamic analyses

The accelerograms obtained after deconvolution have been applied at the bottom of the FEM 3D model (Par. 2.2.) of the bell tower–soil system. These accelerograms have been calculated according to the procedure previously specified, considering the free field conditions of free-field for the elastic layer. However, the presence of the tower modifies the frequency content of the original signal. Therefore, in order to quantify this phenomenon, we performed some specific linear dynamic analyses. These analyses were firstly performed considering only the FE models of the soil and then the complete tower–soil systems (Fig. 11). The results obtained are shown in Fig. 12 in terms of elastic response spectra, calculated for the accelerograms recorded at the surface (point A).

For each component (X, Y, Z) of the considered strong ground motion, it is interesting to compare the original (ITACA working group 2016) elastic response spectra (which coincides with the corresponding accelerogram recorded at surface in free field conditions), with those recorded in the two tower-elastic layer models (Fig. 11). We observe that the presence of the tower causes a variation of the spectral ordinates when compared to the original free field condition, and this indicates a modification of the frequency content of the signal at the base of the tower (Stewart and Fenves 1998; Guéguen and Bard 2005). This variation appears quite small for the x–y acceleration component in the range of the periods of interest, while for the z-component, it is possible to notice an evident alteration of the spectral response. Basically, the tower is characterized by an important mass, while the area of its foundation is relatively small. High frequency signals are absorbed, and this effect is more evident as much as the soil becomes deformable. Farther, the more the soil is deformable, the lower is the minimum threshold frequency because of the less velocity of waves propagation. Therefore, it can be concluded that high frequency waves can pass through the ground-tower interface, while waves with long periods are reflected, as in free field conditions. This result could be also predicted by comparing the frequency responses relative to the axial mode for the cantilever scheme and for the bell-tower–soil system: it can in fact be observed that in the second case the elastic response is reduced.

5.2 Non-linear dynamic analyses

Finally, non-linear dynamic analyses were carried out for the three numerical models previously described (Cantilever scheme; tower on soil I; tower on soil II), adopting for the masonry the constitutive CDP material model described in Par. 2.3.2. This allowed us to evaluate the effects of the deformability of the soil on the seismic damage mechanisms of the tower. The dynamic analyses were performed by considering also the vertical (Z) component of the accelerogram, in order to provide an insight about its influence on the damage scenario.

For each of the two strong ground motions (Gemona and Mirandola), two different load cases were considered for each numerical model: (1) only the X–Y (horizontal) components of the accelerograms are applied; (2) all the spatial components X, Y, Z of the accelerograms are applied.

Figures 13, 14, 16, and 17 report the results obtained in terms of the scalar variable of damage d_t (as defined in Par. 2.3.2). The crushing damage d_c (as defined in Par. 2.3.2) is much less relevant than the cracking one, and thus for the sake of brevity is not reported.

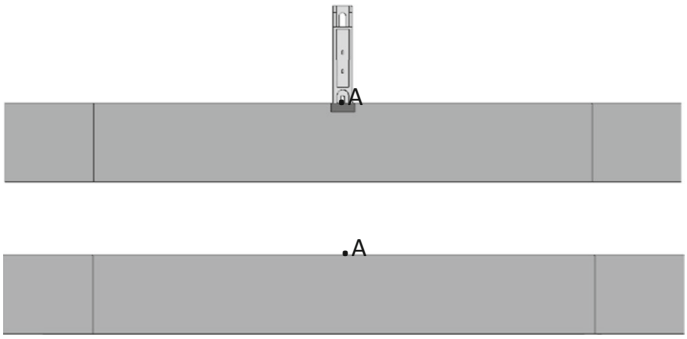

Fig. 11 Reference *point A* on the surface of the individual elastic layer and tower-elastic layer FEM model

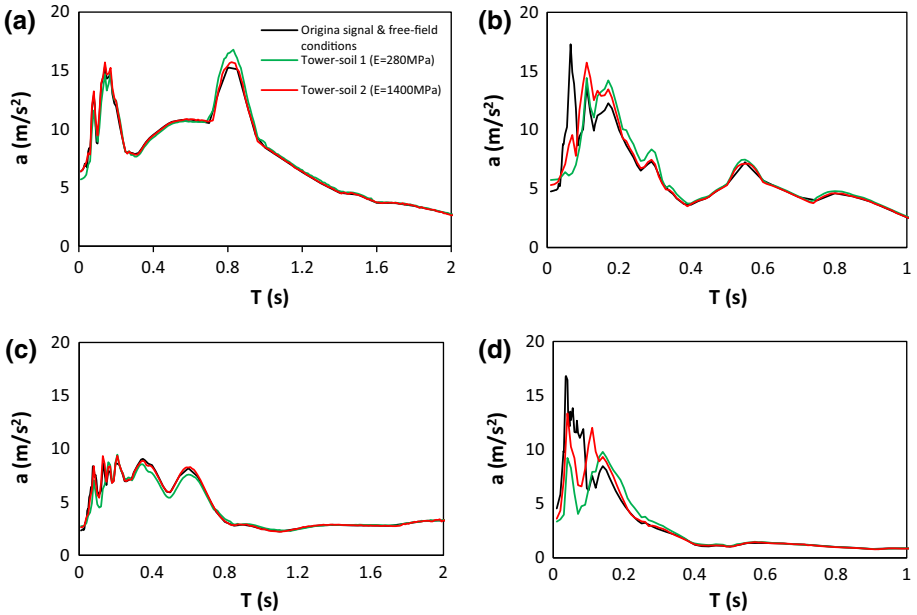

Fig. 12 Gemona accelerogram response spectrum in the X direction (**a**), and in the Z (*vertical*) direction (**b**); Mirandola accelerogram response spectrum in the X direction (**c**) and in the Z (*vertical*) direction (**d**)

Moreover, the damage variable d_c is proved to be also less explanatory of the differences found for the three models (Fig. 15).

The analyses show that the selected strong ground motions lead to the complete collapse of the structure, and thence these figures report the results of the dynamic analyses at a specific time instant, properly chosen in order to display the significant differences in the response of the three models just before the complete collapse.

The tower on soil I (E = 280 MPa) exhibits a localized damage in the lower part of the structure both for Gemona Earthquake and for Mirandola Earthquake. Also the cantilever scheme and the tower on soil II (E = 1400 MPa) show prevalent damage at the base for Gemona Earthquake, while cracks develop also on the top of the tower (at the base of the belfry) for Mirandola Earthquake. It is therefore evident that the accelerogram of

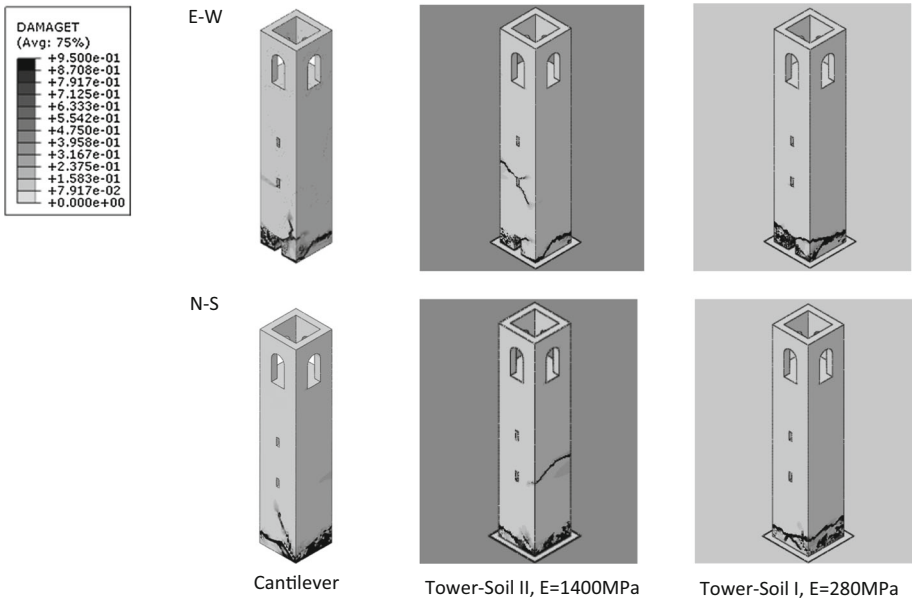

Fig. 13 Strong ground motion of Gemona, NLDA performed with X, Y components (d_t at 5.187 s)

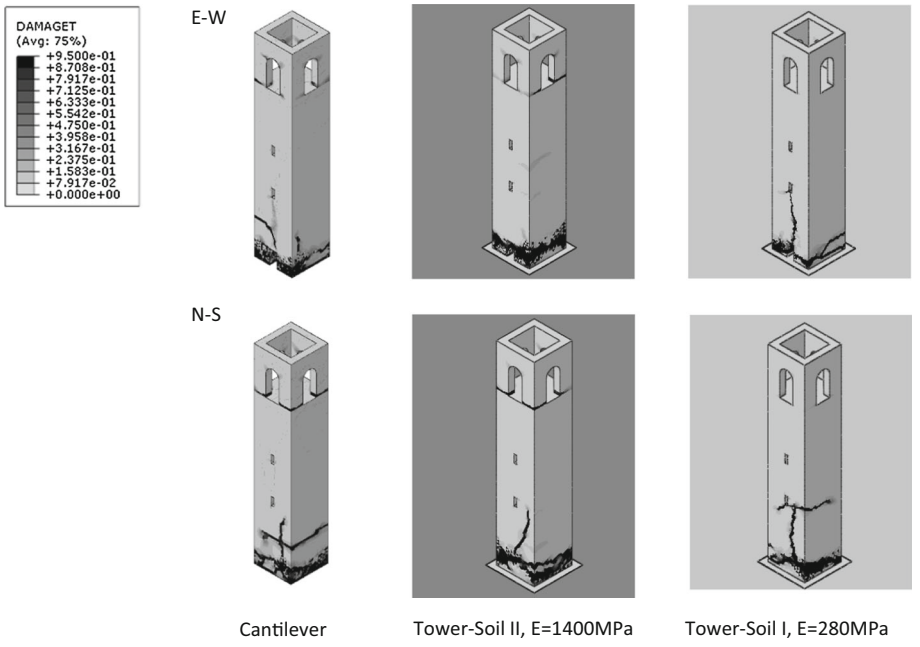

Fig. 14 Strong ground motion of Mirandola NLDA performed with X, Y components (d_t at 9.911 s)

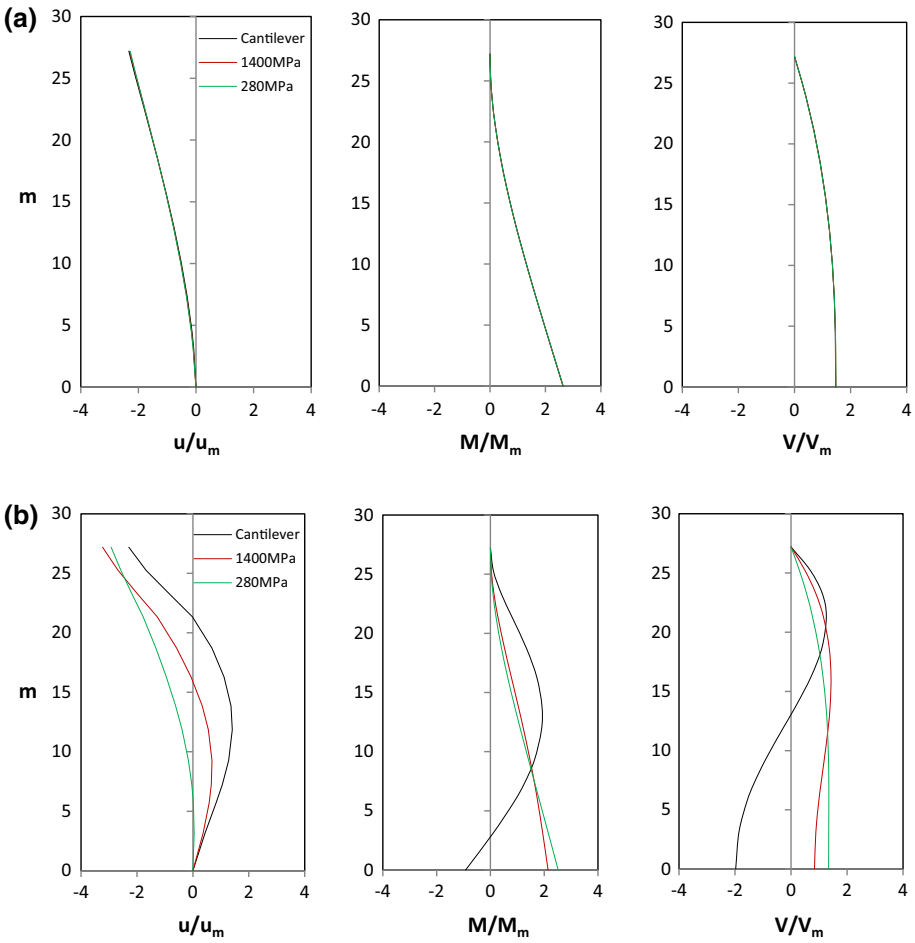

Fig. 15 Transverse displacement **u** (depurated from rigid body motions), bending moment **M** and shear diagrams **V** (normalized by the average of the absolute values $\mathbf{u_m}$, $\mathbf{M_m}$ and $\mathbf{V_m}$) for the 1st natural mode (**a**), and for the 2nd natural mode (**b**)

Mirandola determines a significant excitation of high vibration modes of the tower. This circumstance is partially related to the energy concentration at high-frequencies with respect to that of Gemona.

The excitation of high vibration modes entails different consequences depending on the support at the base of the tower adopted. By considering the shapes of the first and second natural modes depurated from the rigid body motions (rigid translation of the base and rocking values that are shown in Table 8; Fig. 9), one can deduce a shear and bending moment simplified diagrams in order to observe the differences in internal action distribution caused by the different base support of the three models (Fig. 15). As pointed out in Sect. 3, while for the first natural mode, the differences among the three models are almost only in the frequency values, for the second mode, they are also in the modal shapes.

Consequently, for the second mode, the distribution of shear forces and bending moment along the height of the tower is rather different for the three models considered. In

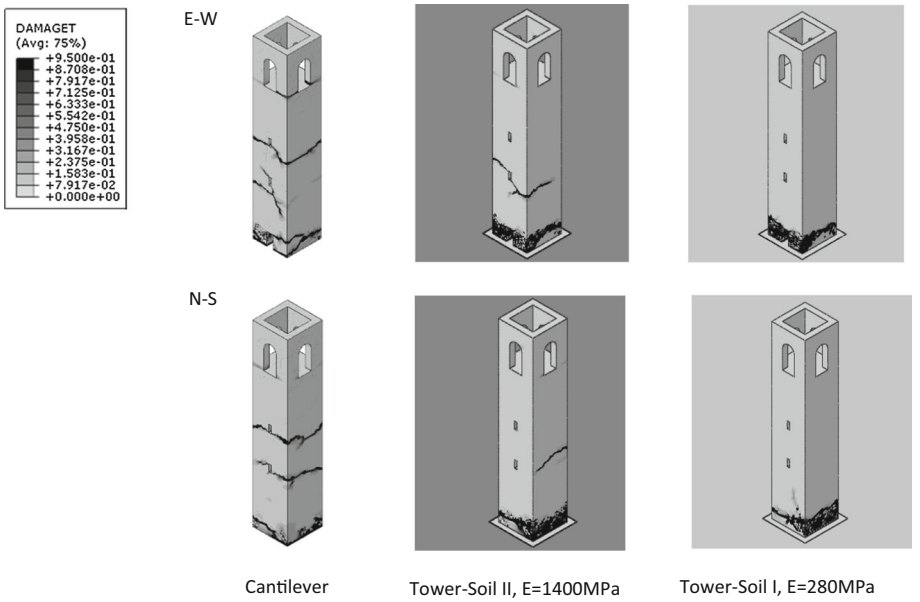

Fig. 16 Strong ground motion of Gemona NLDA performed with X, Y, Z components (d_t at 5.187 s)

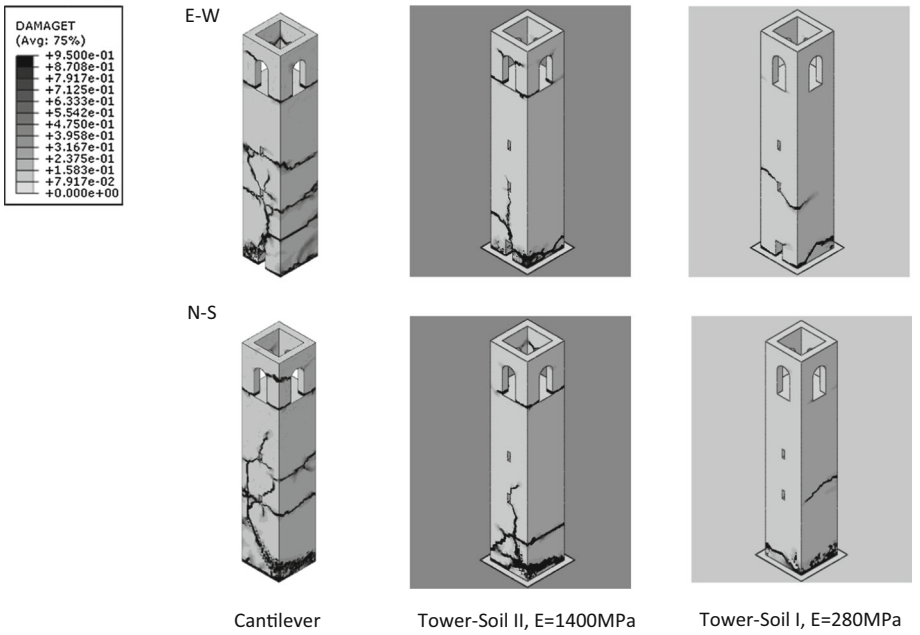

Fig. 17 Strong ground motion of Mirandola NLDA performed with X, Y, Z components (d_t at 9.911 s)

particular, it is worth noting that for the cantilever model and for the tower on soil II, the 2nd mode shear diagram presents a relative maximum in the upper part of the structure, while for the tower on soil I the maximum values are obtained at the base. The damage

observed at the belfry base for the cantilever model and for the tower on soil II under Mirandola Earthquake are related to the concentration of shear stress present in the upper part of the structure (Doglioni et al. 1994; Pintucchi and Zani 2014). Shear stresses are particularly dangerous, in this case, because of the reduction of the normal vertical compression stress component. In fact, the plasticity model adopted is characterized by a pressure dependent yield condition. The cracks observed in the lower part of the tower for both the strong ground motions used and for all the three numerical models are mainly bending damage, related to the principal vibration mode.

By looking at the results of non-linear dynamic analyses with and without the vertical component of the acceleration, it appears that there are little differences in terms of damage, for both the tower on soil I and the tower on soil II. Certainly we can observe that for the tower on soil II, the vertical component of acceleration causes a slight increase of crack patterns severity.

On the other hand, in the case of the cantilever model, the crack pattern resulting by the analyses that consider the vertical component is substantially more significant, with reference to the cracks arising in the central part and at the base of the bell tower. This circumstance can be explained by observing that the presence of the tower causes a reduction of the high frequencies of the seismic signal (with respect to free field conditions), and this reduction is more marked as more the soil is deformable. As a result, there is a modification of the response spectrum of the initial vertical strong ground motion. Moreover, the axial mode frequency value is reduced by a third from cantilever model to tower on soil I model (Figs. 8, 12). The waves that enter into the tower from the base have the possibility to re-cross the border foundation–soil and to propagate back into the soil. In a cantilever model, instead, when the initial vertical accelerogram is assigned at the base of the tower, then the waves undergoes multiple reflections in correspondence of the base determining a more marked damage of the structure.

6 Concluding remarks

Within the scientific community, it is well acknowledged that the dynamic response of slender masonry towers is strongly conditioned by Soil Structure Interaction (SSI). In the presence of a compact rock, of course, it is reasonable to assume a perfectly fixed support at the base, but in most cases it should be expected that these structures (widespread in Italian historical centers) are rather built on softer ground types, such as compact gravel or medium-dense sand deposits.

Starting from these considerations, the paper presents a research study devoted to the appraisal of the relevance of SSI on the dynamic response and damage scenarios of a typical masonry bell-tower, by a fairly accurate 3D FEM modeling that includes a significant volume of soil discretized by means of infinite elements (soil I and soil II). Specific attention has been also devoted to the influence of the vertical acceleration on damage mechanisms, and to the alteration induced by the presence of the tower on the frequency content of the signal recorded on the surface with respect to free-field condition. It has been observed that the presence of the soil has little influence on the first natural frequency and the corresponding modal shape, which is almost totally preserved. The second mode, instead, is deeply modified both in frequency and in shape. More in detail, in the case of soil II, the second mode retains some of the characteristic features of the cantilever model, whereas in the case of the tower on soil I there is almost no correspondence. This is

confirmed by the MAC values obtained for the three models adopted. Hence the second natural mode of the tower is influenced by soil deformability much more than the first one. The alteration of the second modal shape due to SSI is an important aspect that significantly affects the non-linear behaviour of historical towers. When actual natural modes are consistent with the ideal modes corresponding to the cantilever scheme, there is an higher possibility of dangerous concentrations of shear stress in the upper part of the structure. In fact, if the exciting accelerograms do have a sufficient energy content at the second modal frequency, important damage at the belfry level will occur. On the contrary, the increase of soil deformability reduces the damage at the belfry level but determines a damage localization at the base of the tower.

As regard to the influence of the vertical component of the seismic action, it was found that the stiffer is the soil (base constraint scheme becomes closer to a fixed support), the more evident are the differences of the dynamic structural response. This can be explained by observing that the presence of the tower significantly modifies the signal frequency content with respect to free field condition.

The research study presented has clearly shown that the assumption of a fixed base constraint for the structural typology of slender masonry towers is very likely to be unreliable, except that for the case of very stiff soil. In order to provide a realistic prediction of damage scenarios, it is thence recommended the resort to non-linear dynamic analyses which should include significant portion of deformable soil into the model.

References

ABAQUS (2014) ABAQUS documentation version 6.14. Dassault Systèmes, Providence, RI

Acito M, Bocciarelli M, Chesi C, Milani G (2014) Collapse of the clock tower in Finale Emilia after the May 2012 Emilia Romagna earthquake sequence: numerical insight. Eng Struct 72:70–91

Allemang RJ, Brown DL (1982) A correlation coefficient for modal vector analysis. In: Proceedings, international modal analysis conference, pp 110–116

Barbieri G, Biolzi L, Bocciarelli M, Fregonese L, Frigeri A (2013) Assessing the seismic vulnerability of a historical building. Eng Struct 57:523–535

Bartoli G, Betti M, Vignoli A (2016) A numerical study on seismic risk assessment of historic masonry towers: a case study in San Gimignano. Bull Earthq Eng 14:1475–1518

Binda L, Gatti G, Mangano G, Poggi C, Sacchi Landriani G (1992) The collapse of the civic tower of Pavia: a survey of the materials and structure. Mason Int 6(1):1–20

Burban A, Maity D, Sreedeep S (2010) Iterative analysis of concrete gravity dam-nonlinear foundation interaction. Int J Eng Sci Technol 2(4):85–99

Camata G, Cifelli L, Spacone E, Conte J, Torrese P (2008) Safety analysis of the bell tower of Santa Maria Maggiore Cathedral in Guardiagrele. In: WCEE, the 14th world conference on earthquake engineering, Beijing, China

Casolo S (1998) A three-dimensional model for vulnerability analysis of slender medieval masonry towers. J Earthq Eng 2(4):487–512

Casolo S, Uva G (2013) Non-linear dynamic analysis of masonry towers under natural accelerograms accounting for soil-structure interaction COMPDYN 2013. Kos Island, Greece

Casolo S, Milani G, Uva G, Alessandri C (2013) Comparative seismic vulnerability analysis on ten masonry towers in the coastal Po Valley in Italy. Eng Struct 49:465–490

Clayton RW, Wiggins RA (1976) Source shape estimation and deconvolution of teleseismic bodywaves. Geophys J Int 47(1):151–177

Curti E, Lagomarsino S, Podestà S (2006) Dynamic models for the seismic analysis of ancient bell towers. In: Lourenço PB, Roca P, Modena C, Agrawal S (eds) Proceedings of structural analysis of historical constructions SAHC. MacMillan, New Delhi

Doglioni F, Moretti A, Petrini V (1994) Le Chiese e il Terremoto. Lint Press, Trieste

Gentile C, Saisi A, Cabboi A (2015) Structural identification of a masonry tower based on operational modal analysis. Int J Archit Herit 9(2):98–110

Giresini L (2016) Energy-based method for identifying vulnerable macro-elements in historic masonry churches. Bull Earthq Eng 14:919–942
Guéguen P, Bard PY (2005) Soil-structure and soil-structure–soil interaction: experimental evidence at the Volvi test site. J Earthq Eng 9(5):657–693
ITACA Working Group (2016) ITalian ACcelerometric Archive, version 2.1. doi:10.13127/ITACA/2.1
Ivorra S, Pallares FJ (2006) Dynamic investigations on a masonry bell tower. Eng Struct 28:660–667
Ivorra S, Pallarés FJ, Adam JM, Tomás R (2010) An evaluation of the incidence of soil subsidence on the dynamic behaviour of a Gothic bell tower. Eng Struct 32(8):2318–2325
Ivorra S, Brotóns V, Foti D, Diaferio M (2016) A preliminary approach of dynamic identification of slender buildings by neuronal networks. Int J Non-Linear Mech 80:183–189
Kouroussis G, Verlinden O, Conti C (2011) Finite dynamic model for infinite media: the corrected solution of viscous boundary efficiency. J Eng Mech
Kramer SL (1996) Geotechnical earthquake engineering (Prentice-Hall international series in civil engineering and engineering mechanics). Pearson Education
Kuhlemeyer RL, Lysmer J (1973) Finite element method accuracy for wave propagation problems. J Soil Mech Found Div Am Soc Civ Eng 99(SM5):421–427
Lee J, Fenves GL (1998) A plastic-damage model for earthquake analysis of dams. Earthq Eng Struct Dyn 27:937–956
Lourenço PB (2002) Computations of historic masonry constructions. Prog Struct Eng Mater 4(3):301–319
Lubliner J, Oliver J, Oller S, Onate E (1989) A plastic-damage model for concrete. Int J Solids Struct 25(3):299–326
Luco JE, Trifunac MD, Wong HL (1988) Isolation of soil-structure interaction effects by full-scale forced vibration tests. Earthq Eng Struct Dyn 16(1):1–21
Luzi L, Hailemikael S, Bindi D, Pacor F, Mele F, Sabetta F (2008) ITACA (ITalian ACcelerometric Archive): a web portal for the dissemination of italian strong-motion data. Seismol Res Lett 79(5):716–722
Lysmer J, Kuhlemeyer RL (1969) Finite dynamic model for infinite media. J Eng Mech Div ASCE Am Soc Civ Eng 95(EM4):859–877
Milani G, Valente M (2015) Failure analysis of seven masonry churches severely damaged during the 2012 Emilia-Romagna (Italy) earthquake: non-linear dynamic analyses vs conventional static approaches. Eng Fail Anal 54:13–56
Milani G, Valente M (2016) Non-linear dynamic and static analyses on eight historical masonry towers in the North-East of Italy. Eng Struct 114:241–270
Milani G, Casolo S, Naliato A, Tralli A (2012) Seismic assessment of a medieval masonry tower in Northern Italy by limit, non-linear static and full dynamic analyses. Int J Archit Herit 6(5):489–524
Pacor F, Paolucci R, Luzi L, Sabetta F, Spinelli A, Gorini A, Nicoletti M, Marcucci S, Filippi L, Dolce M (2011) Overview of the Italian strong motion database ITACA 1.0. Bull Earthq Eng 9(6):1723–1739
Pena F, Lourenço PB, Mendez N, Oliveira D (2010) Numerical models for the seismic assessment of an old masonry tower. Eng Struct 32:1466–1478
Pintucchi B, Zani N (2014) Effectiveness of nonlinear static procedures for slender masonry towers. Bull Earthq Eng 12:2531–2556
Stewart JP, Fenves GL (1998) System identification for evaluating soil-structure interaction effects in buildings from strong motion recordings. J Earthq Eng Struct Dyn 27:869–885
Van Der Pluijm R (1993) Shear behavior of bed joints. In: Proceedings of the 6th North American Masonry conference, pp 125–136
Veletsos AS, Meek JW (1974) Dynamic behavior of building foundation systems. J. Earthq Eng Struct Dyn 3(2):121–138
Yerli HR, Kacin S, Kocak S (2003) A parallel finite–infinite element model for two dimensional soil-structure interaction problems. Soil Dyn Earthq Eng 23:249–253
Zienkiewicz OC, Emson C, Bettess P (1983) A novel boundary infinite element. Int J Numer Methods Eng 19(3):393–404
Zienkiewicz OC, Bando K, Bettes P, Emson C, Chiam TC (1985) Mapped infinite elements for exterior wave problems. Int J Numer Methods Eng 21(7):1229–1251